JLC X-BAND TECHNICAL NOTE

Improved HDDS cell fabrication for H60VG3S18

T. Higo, Y. Funahashi, Y. Higashi, N. Hitomi, N. Kudoh, T. Kume, Y. Morozumi, K. Takata,

T. Takatomi, N. Toge and Y. Watanabe

* KEK, High Energy Accelerator Research Organization

1-1, Oho, Tsukuba, Ibaraki, 305-0801, Japan

Abstract

Based on the fabrication experience of 45mm-diameter HDDS cells, the cell fabrication for the H60VG3S18 structure was improved in many aspects. In the present paper are described those improved methods by showing the measured characteristics of the H60VG3S18 cells.   The tangential-angle discontinuities between two surfaces shaped by multiple processes were stably suppressed within specified values. Dimensions, which determined the cell frequency, were found also well controlled. Here are shown some of the typical results of the dimensional and electrical inspections.

1. Introduction

In a previous report[1], the first HDDS cell fabrication was described. There, the cell outer diameter was 45mm and the number of cell production was only 6. Since the structure had to be tested with a minimum preparation time, these cells were made before completely establishing the fabrication process. One of the problems left is the tangential discontinuity between two surfaces, especially the junction between milled surface and turned one. We were not sure whether the angle was within a specified value. Another problem is the poor flatness of the end surface.

As the next step, the first full HDDS structure, H60VG3S18, was planned to really study the HDDS scheme in a practical manner[2]. Here all of the cells in the structure were composed of HDDS cells with their diameter 61mm. Based on the experience of 45mm cells, various improvements were made and applied to the present cells. In the present note are described these improved fabrication processes with the inspection results.

2. Cell shape and specifications

The cell cross section is shown in Fig. 1. One of the main differences is the diameter, now 61mm. All other dimensions are the same as before. Some tighter tolerances are specified on manifold shape, where some details are shown in Fig. 2. The specifications on the tangential discontinuity angles are the same as before and listed in Table 1.
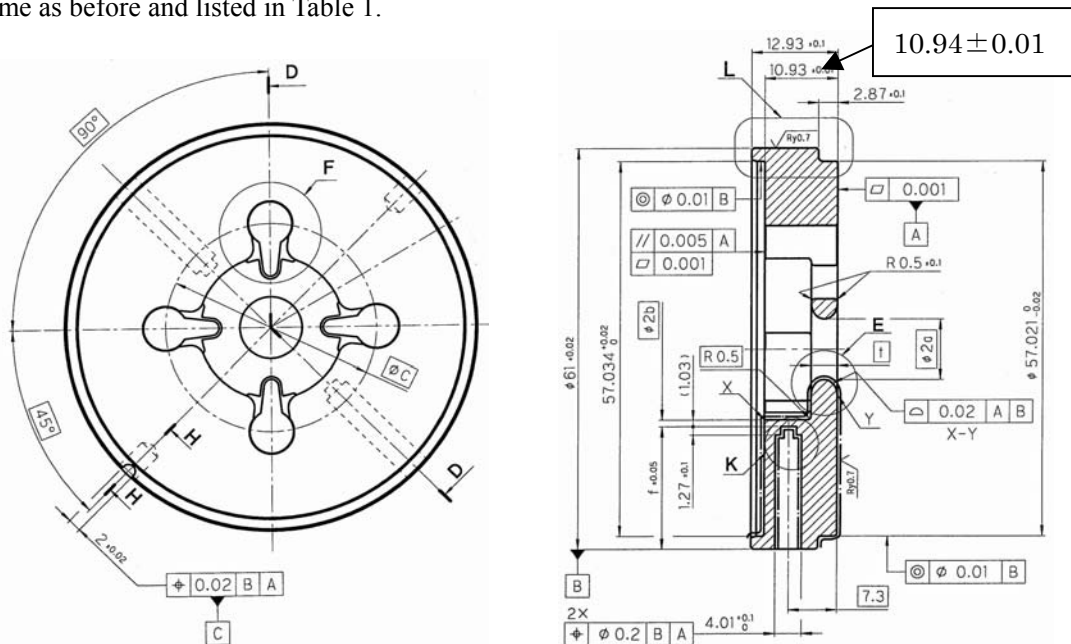

Fig. 1. Cutout of the cell drawing. Cell is 10 μm thicker than nominal to leave the amount of final cut at KEK.

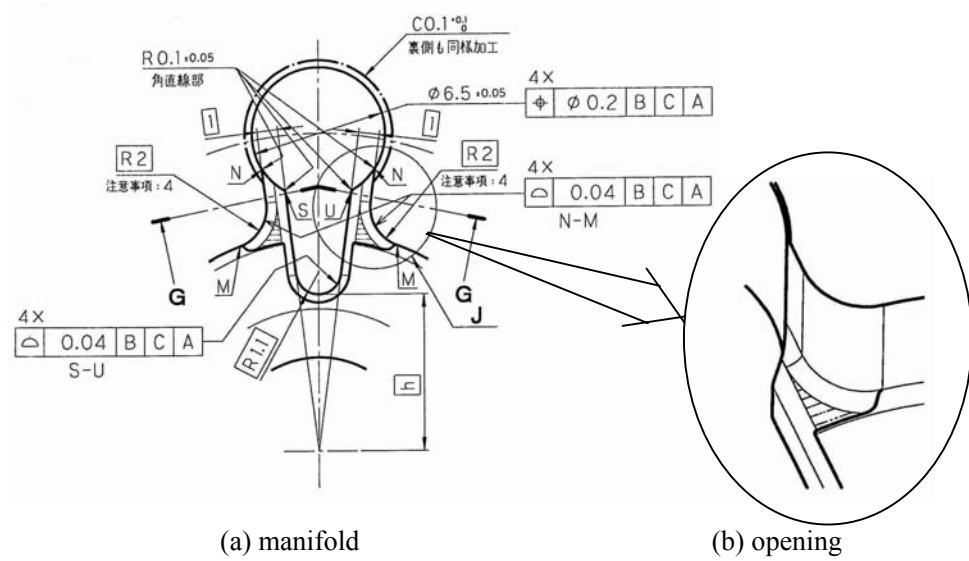(a) manifold   (b) opening

Fig. 2.   Manifold detail view; (a) manifold and (b) close-up of the opening seen from cell to manifold showing the step between turned surface and milled base surface.

Table 1. Specification of tangential discontinuity between two surfaces.

	Junction	Angle
(a)	"2b—r2"	< 5 degrees
(b)	"r0.5—flat"	< 12 degrees
(c)	"ellipse—flat"	< 1 degree

Requirement of flatness of end surfaces:

The end surfaces of the previous HDDS cells were not good enough for the diffusion bonding. Therefore, the flatness of the present cells was to be improved and it was specified to be 0.5 μm or better.

3. Fabrication method

Even if introducing the better lathe, it did not use a vacuum chuck but used a diaphragm chuck, which grabbed a cell at the outside diameter with radial force, the resulting flatness was sometimes as bad as one micron. Therefore, we decided to cut end surfaces with a single-crystal diamond turning at KEK as the final step of the fabrication. This cut would make the flatness over the bonding surface better than 0.5 μm. The typical fabrication flow is shown below, where the changes added to the present fabrication are shown by underlines.

Fabrication steps:

1. Cut disk from bar stock

2. Rough turning with 0.2mm—0.5mm undercut

4. Annealing at 500C for 1 hour

5. Boring tuning holes

6. Turning cup side to its final dimensions

7. Turning disk side with undercut by 10—20 μm

8. Measurement of relevant dimensions

9. Milling cup side including HOM manifolds and slots

10. Milling disk side for rounding the slot edge

11. Turning cup-side end surface

12. Turning with tool fixed at r=a and moving in Z-direction passing over "2a" point

13. Turning disk-side end surface and cell inside toward "2a" point

14. Rinsing in an isopropyl-alcohol bath with ultra-sonic vibration

15. Drying by blowing with nitrogen gas

16. Deliver to KEK

17. Inspection of junction angle at (b) and (c)

18. Single-crystal diamond turning for both bonding surface

19. Check flatness of both end surfaces

20. RF inspection on a floating setup

21. Shipping to SLAC

Tool shape to control the tangential discontinuity (b):

The suppression of the discontinuity angle (b) between the radius 0.5mm and flat surface of the cup side was improved by adopting suitable tool shapes as shown in Fig. 3. In order to relax the tolerance on the axial positioning of milling tool, the tool escape angle θ was increased from 3 degrees to 8 degrees, still less than the specification of 12 degrees, but keeping the extension amount β to be 50 μm. This changes the tolerable range of the axial positioning of the milling tool with respect to the nominal position from a few μm in 3 degree case to more than 10 microns in 8 degree case, as listed in Table 2. Using this tool, the angle in the cup-side was well controlled because the milling tool position can be adjusted well based on the checking of the turned surface, which is already cut to its final position. However, when the milling of the radius 0.5mm on slot edge of the disk-side surface is performed, the surface is still undercut by 10-20 micron leaving for later turning. Therefore, it is not easy for the company to precisely position the milling tool in its axial direction

with respect to the disk surface, which is shaped later with a lathe of a limited positioning control in the thickness direction. Then we decided to adopt a fat milling tool by extending the part with a relief angle outward from $\beta=50\mu m$ to $250\mu m$, which makes the tolerable range of the tool positioning to $40\mu m$ apart from the nominal surface even in one direction. This special tool was used only for shaping the slot edges of the disk side.
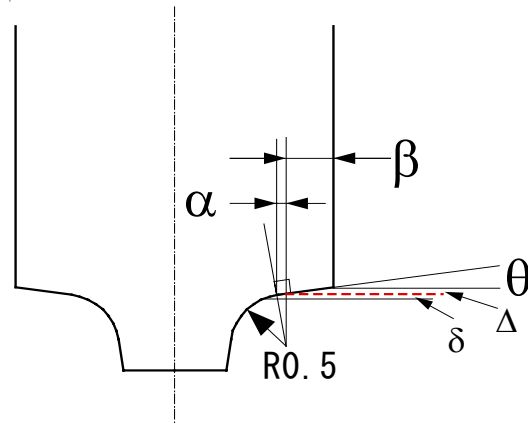

Fig. 3. Milling tool for rounding slot edge with a radius 0.5mm. Nominal position is the tool outer edge position when $\alpha=\beta=\theta=0$ indicated by dashed line. δ is the position difference at an angle of 12 degrees from the nominal position. Δ is the position difference of outer edge of the tool from the nominal position.

Table 2. Dimensions of milling tool.

Structure to be fabricated	Side	θ (degrees)	β (μm)	δ	Δ
H60VG3N-6C (ϕ 45mm)	Both sides	3	50	11	3
H60VG3S18 (ϕ 61mm)	Cup side	8	50	11	12
	Disk side	8	250	11	40

Tool path to form the junction (a):

The tolerance on the relative positioning between milled circle with $r_M=2mm$ and the turned circle with $r_L=b$ was only $-6\mu m$ and $+4\mu m$ for the case of $r_E=3mm$[1]. We found that the careful milling will remove the scissel problems at the junction so that the escape circle radius r_E can be increased to close to"b". We actually set at $r_E=9mm$. In this case the relative tolerable positioning is between $-6\mu m$ to $+100\mu m$ to make the junction angle less than 5 degrees as shown in Fig. 5. Thus the positioning tolerance is greatly enlarged, though only in positive side, i.e. the direction of two circles to be separated more. Even adopting this passage, the tool path in the present fabrication was not intentionally offset towards positive side, taking the advantage of the good milling skill and good "2b" control of turning in dimension and mutual positioning.
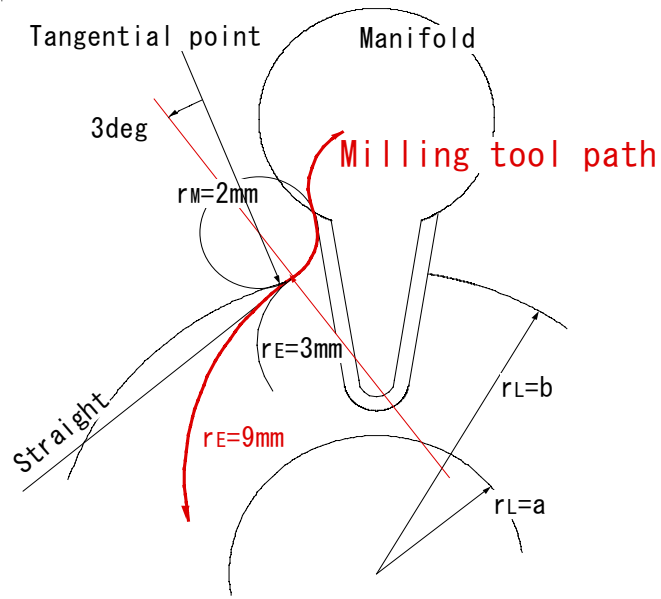
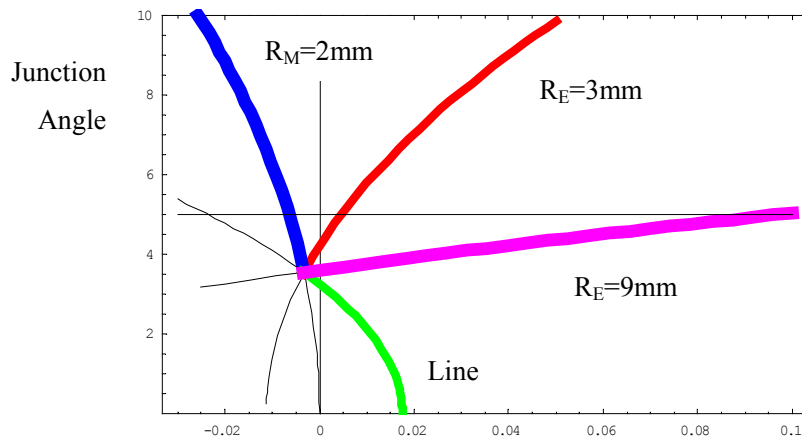Fig. 4.   Milling tool path shown in red line for "2b—r2".

Fig. 5. Dependence of tangential discontinuity at (a) "2b—r2" on relative positioning error between turning and milling. Pink line shows the case with the escape circle of radius 9mm, while red line the case with escape radius 3mm and green line the case escaping in a straight line. The blue line shows the case intersecting between turned surface "2b" and milled surface with a radius 2mm.

Improvement of end surface flatness:

The bonding surface was cut at the last stage with a single-crystal diamond turning by KEK to make the surface flatness better than 0.5 μm. The cut surfaces are schematically shown in Fig. 6. The cutting amount at each side is nominally 5 μm. The disk side was cut down to the point where the tool center is radially located 50 μm inner than the "b" of the next cell. This keeps the inner side of each cell as machined by the vendor company so that the surface quality inside a cell is totally

determined by the fabrication of the vendor company. The cup side end surface was cut from "b" to the outer most point where the tool with its radius 0.4mm nearly touches to the radius 0.5mm of the corner made in the previous process. This ensure the clearance from the other side with radius 0.6mm.
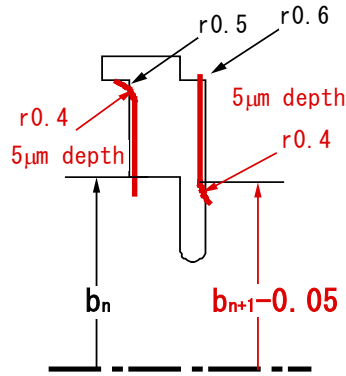

Fig. 6.   Final diamond turned surface shown in red.

4. Results on mechanical characteristics of cells

Flatness:

Flatness of each cell was inspected by an interferometer, FUJINON F601[3] after final cutting at KEK. Some of the cell showed huge amount of flatness value but we believe that these were picking up the local tiny peaks so that it does not mean very bad surface for bonding. Since we lost the file recording the measured detailed pattern, these bad cells whose flatness are more than 0.5 μm or so should be checked again before bonding.
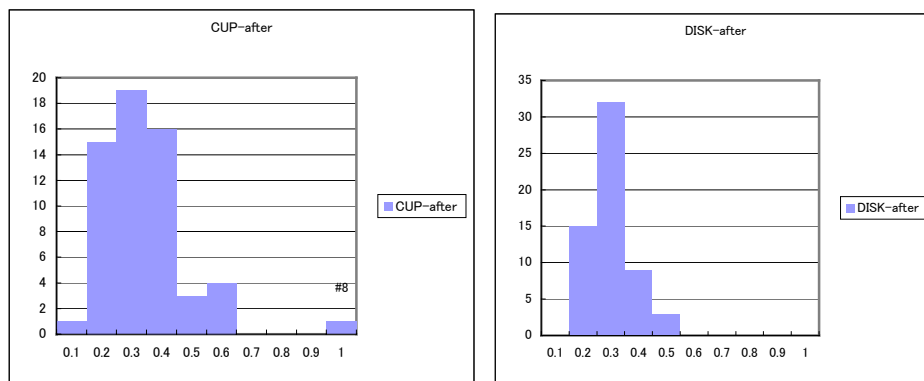

Fig. 7. Statistics of the flatness of bonding surface after diamond turning at KEK.

Surface roughness:

   The surfaced roughness of the cup side was the same as before (H60VG3N-6C), because no change in its fabrication process, with turning by MORI-SEIKI lathe. It is shown in Fig. 8 as a reference[1]. However, that of the disk side changed because of the application of the new lathe of SEIBU-DENKI. The surface roughness was measured using the same machine as before, Mitsutoyo, Formtracer CS-5000, using 5μm probe at 4mN pressure.[4] Typical result is shown in Fig. 9. Roughness on flat surface Ra is 0.02μm and Ry 0.12μm. The quality was improved much comparing to the previous shown in Fig. 8.   The roughness on elliptical surface shows a worse value but still better than before. The steep step at the right hand side is probably due to the error in centering between cuttings from both sides. The lathes used for various surfaces machining are summarized in Table 3.

   In summary, we need to remind this surface difference between cup side and disk side when we find any difference between the two sides in high power performance.
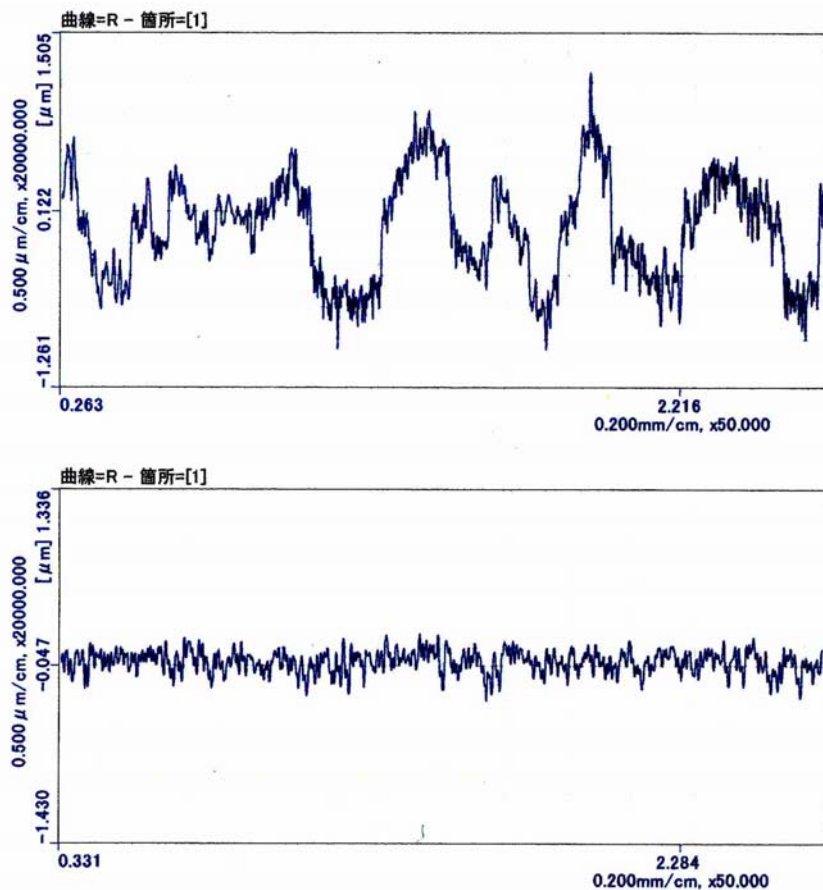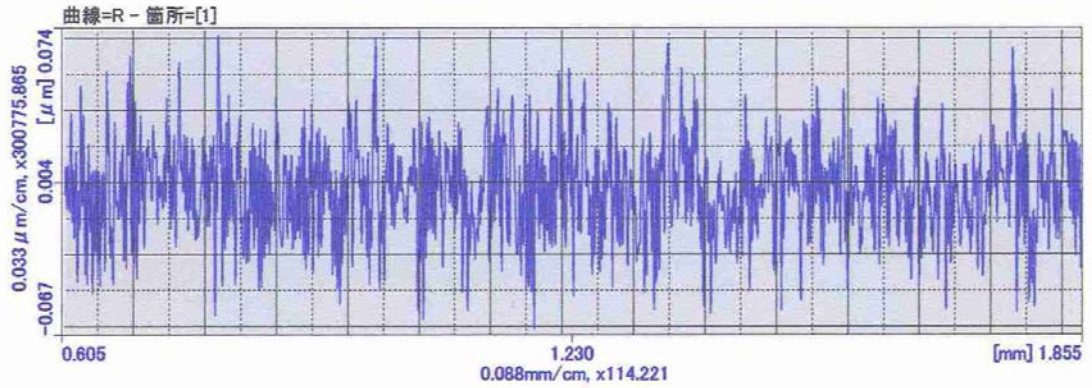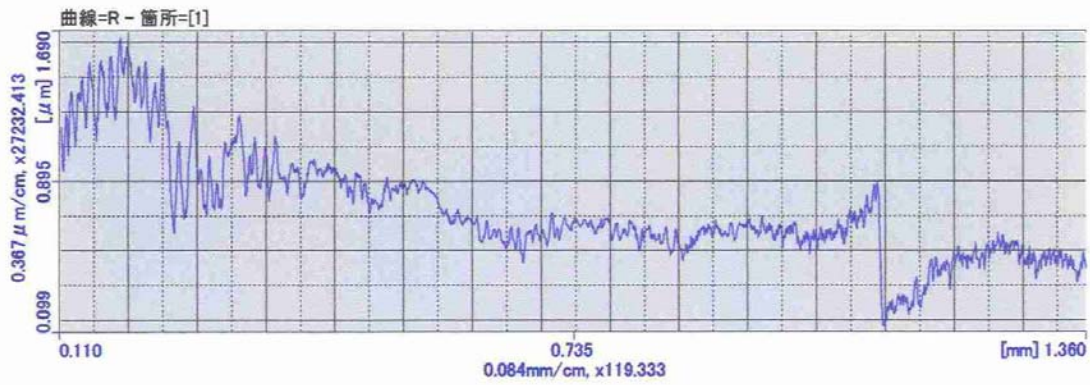

Fig. 8. Roughness of turned surface by MORI-SEIKI lathe in the previous structure, H60VG3N-6C. Upper is on the elliptical surface while lower on a flat part.

8

(a) Flat part. Horizontal span is 1.2mm, while vertical about ±0.07μm.

(b) Elliptical part. Horizontal span is 1.2mm, while vertical about ±1.6μm.

Fig. 9.   Roughness of turned surface cut by the new SEIBU-DENKI lathe.

Table 3. List of the lathes, which were used for the cutting of each part of a cell. M: with a lathe of MORI-SEIKI co., S: with a lathe of SEIBU-DENKI co. and K: single-crystal diamond turning by KEK.

	H60VG3N-6C	H60VG3S18
Cup-side cell inside	M	M
Disk-side cell inside	M	S
Cup-side end surface	M	K
Disk-side end surface	M	K

Inspection of tangential discontinuity (b):

     We realized that the marking due to tracing by Mitsutoyo, Formtracer[4], to check the junction angle at (b) and (c) must not be harmful on high-field performances. This idea is based on the understanding that the depth of the trace is much less than roughness of the lathe so that the depth is also much less than the amount of the etching depth, typically 3 μm or so. Here we use the

9

scanning using a probe with its diameter 0.5mm and with pressure at 4mN during the scanning. Since the trace can be made without cutting the cell, we inspected all of the production cells. The typical measured cross sectional shape is shown in Fig. 10. As shown in the figure, the slope at 8 degrees appeared with intersecting to the flat surface at the same angle. We confirmed that the angles were 8 degrees in all of the production cells. The inspection was performed along a single radial line of each side of a cell. The line is from the axis to randomly chosen one of the four manifolds shown in Fig. 2 (a).
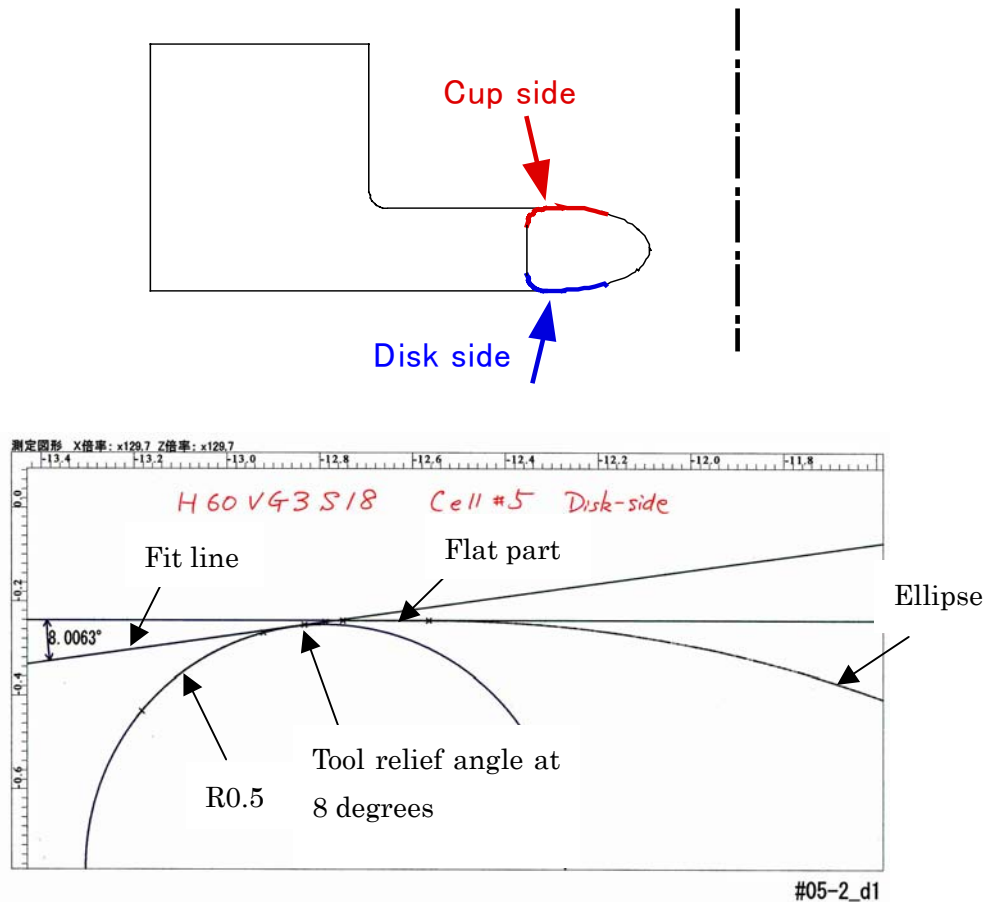

Fig. 10. Measurement of angle of junction at (b), "r0.5—flat". Top schematic cross section shows the line to be measured. Bottom shows the actual measured data with fit curves overlayed. This case clearly shows the slope at 8 degrees.

Inspection of tangential discontinuity (a):

Even if using the same condition of probing as the part (b) and (c), the inspection at (a) without cutting is not easy, though in principle possible. Since the yielding rate at the suppression of the junction angle at (a) became high, we decided to check only some of the duplicate cells, where the cells were cut into half to measure the part (a) in a simpler setup. Typical example is shown in Fig. 11.
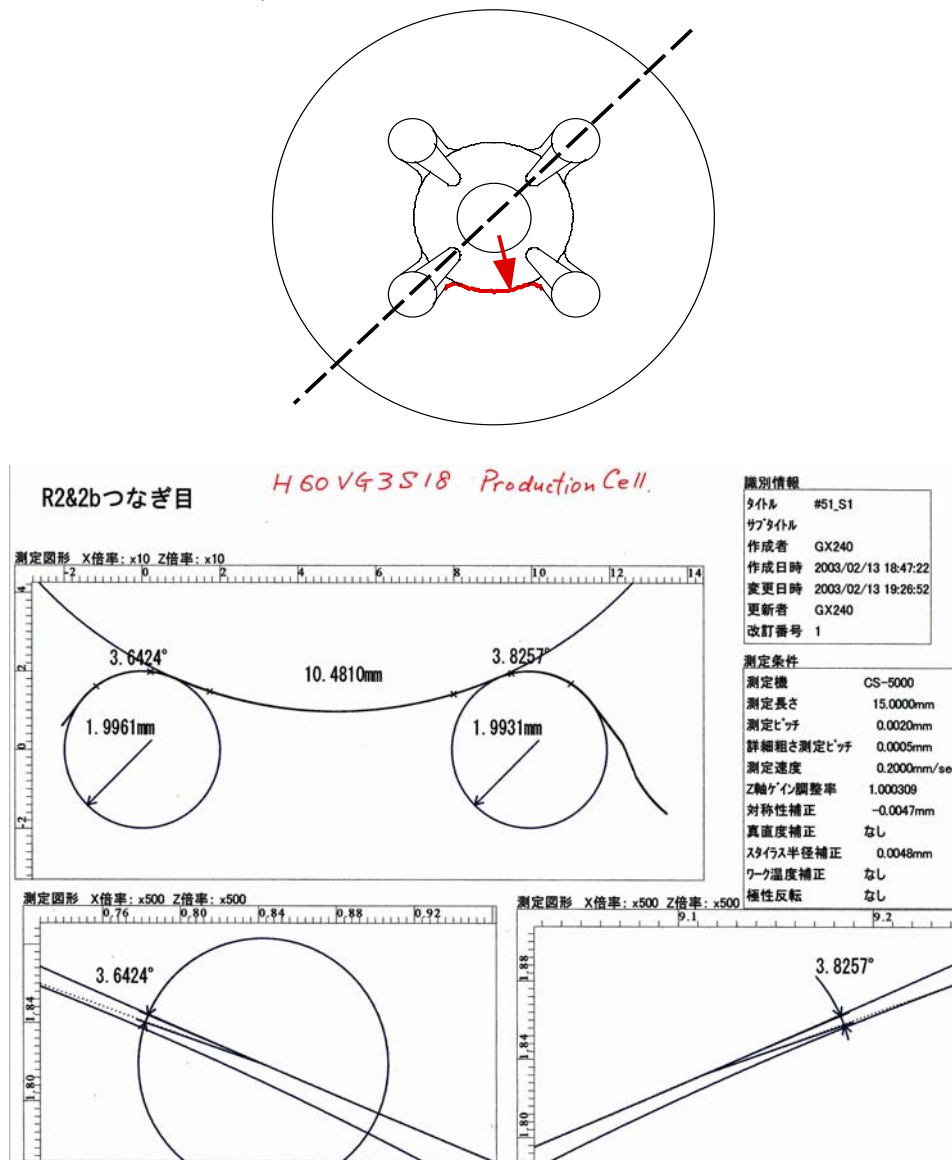
10

Fig. 11. Junction at (a), "2b—r2". Top view shows the cut line and the line to be measured. Bottom line is one of the typical results, where we read these both a little less than 4 degrees.

Table 4. List of estimated angle discontinuities in actual production cells.

Place	Specification	Angle	Measured cells
(a) "2b—r2" *	< 5°	3—4°	Duplicate cells at #3, #15, #51
(b) "r0.5—flat"	< 12°	7—9°	All cells
(c) "ellipse—flat"	< 1°	< 1°	All cells

From all of these measurements on (a), (b) and (c), we estimate the tangential discontinuity angles in the present structure are below the specification as summarized in Table 4.

Milled surface left inside a cell:

The milling tool moves along the path shown in Fig. 4 to make the opening between cell and manifold. While moving from an opening to the next one by going through the path near "2b", the milled base surface bites into the cell surface for some cells. This happened in the cell #8, #45 and #48. This surface was inspected by a laser microscope [5], as shown in Fig. 12. The height difference was much less than 1 μm and surface roughness of the milled surface was actually better than turned area. Therefore, we concluded that this milling mark was not harmful in high power operation so that we left them as they were.
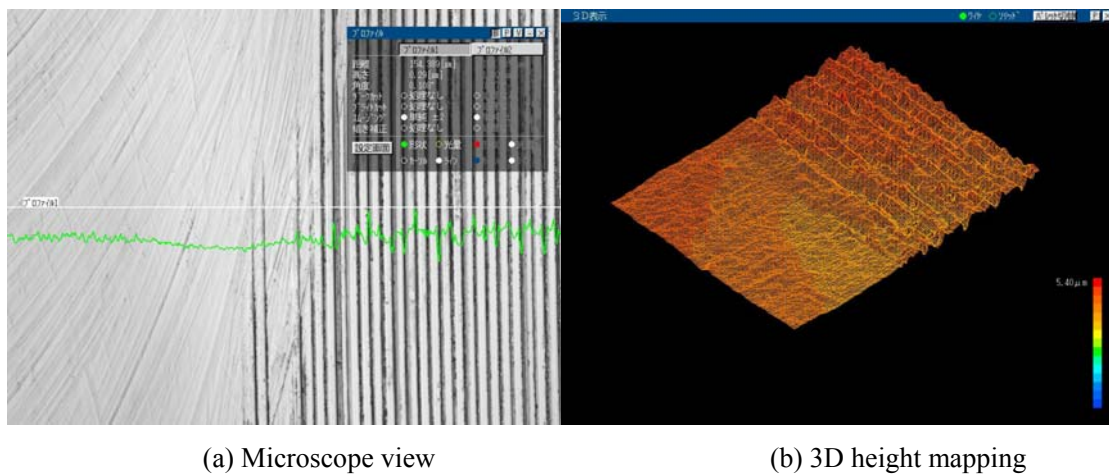

(a) Microscope view   (b) 3D height mapping

Fig. 12.   Milled surface marked on the turned surface. The left half is milled surface and the right half the turned one.

Dimensions of actual cells:

Relevant dimensions such as beam hole diameter "2a", cell diameter "2b", cell thickness "p", slot width "W1", slot position "h", width between r=2mm walls "W3", etc. were measured at the vendor company before shipping to KEK. "2a" was measured by an optical microscope, "2b" by 3D CMM and "p" by a height gauge. The dimensions related to milling on slots and manifolds were measured by an optical microscope. These values were once checked with the CMM inspection at KEK and both agreed within several microns. We understand that the precision of several microns is good enough for the present structure equipped with ±20MHz tuning mechanism so that we fully rely on the measurement by the company except for a few duplicate cells as one of the confirmation purpose.

Typical measurement results are shown in Figs. 13 and 14. As shown in Fig. 13, the dimensions of the turned geometries were controlled within the tolerances of ±20μm. On the other hand, what influences the accelerating mode frequency from milling is the average values at four locations. If

we make averages of the relevant milled dimensions, such as width "W1" and "W3" and position "h", the measured values were found to be controlled within ±10 μm. This is the state of the art of the vendor company as of now.

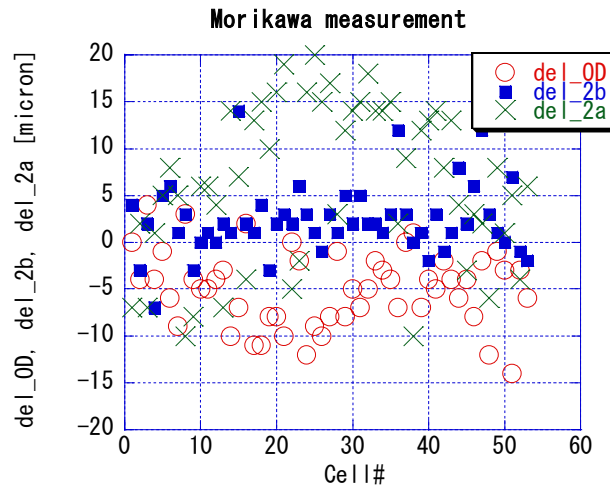These qualities are important to be referred for the further R&D toward controlling dipole mode frequency in future.

Fig. 13. Deviation of measured diameter values from nominal ones. "OD" is the outside diameter, "2a" beam hole diameter and "2b" cell diameter.
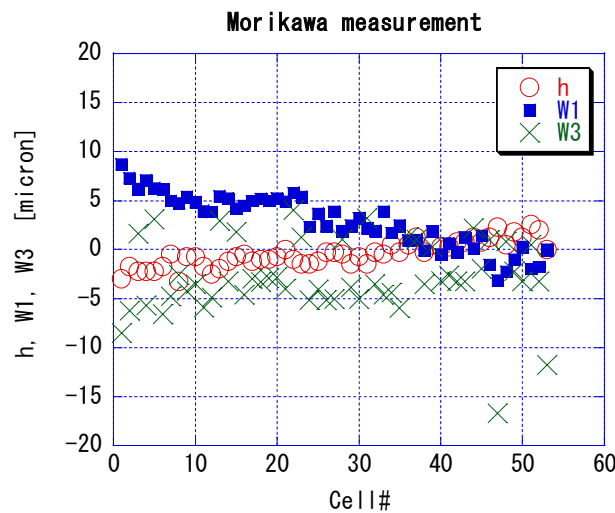

Fig. 14. Deviation of the milled dimensions from nominal ones. "h" is the distance from beam axis to the nearest point of the slot, "W1" the width of slot at r="b" and "W3" the width between two walls with radius 2mm which form the channel between cell and manifold.

5. RF measurement result

RF test characteristics:

The stack measurement was performed for standard cells sandwiched by half cells made by company. As shown in Fig. 15, the measured frequency converged above 300kg within 0.1MHz. Then, we chose the nominal pressure of 350kg for the measurement. This convergence indicates the improved flatness even before KEK's final cut on end surfaces.
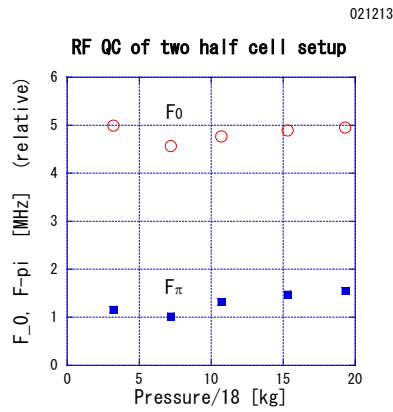

Fig. 15 Frequency characteristics versus total pressure.

Frequency scattering:

Frequency of each cell was checked by the smoothness from cell to cell. Fig. 16 shows the measured frequencies of the F_{2a} and F_{2b}. Fig. 17 shows the deviation from a smooth fitting with a cubic polynomial. Except for the special cells, #1 and #53, the RMS deviation of F_{2a} is 2 MHz and that of F_{2b} 4 MHz. These are much smaller than the tuning range but the maximum deviation is 10 MHz in F_{2b}. Even we admit that this maximum deviation is a little large, we concluded that all of the cells are in the tuning range of $\pm$20MHz.
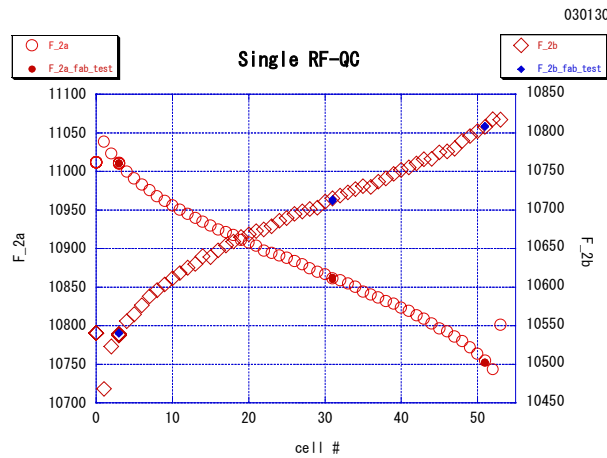

Fig. 16. F_{2a} and F_{2b} frequencies of the production cells.

Single RF-QC of H60VG3S18
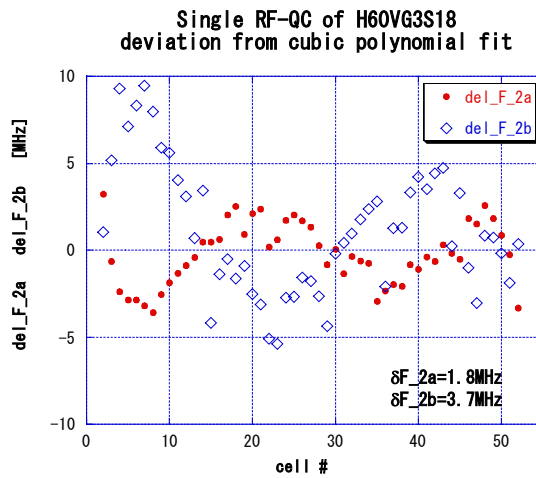deviation from cubic polynomial fit

Fig. 17.   Deviation from the fit with a cubic polynomial in Fig. 16.

Absolute frequency estimation:

In order to get the absolute frequency of the accelerating mode, the $5\pi/6$ mode frequency with (N-1) cells inserted between two half cells was obtained by fitting the dispersion curve. The value for the periodic structure was obtained by changing the N as shown in an example of Fig. 18. The obtained actual resonant frequencies at 45 degrees C in vacuum are listed in the Table 3. The correction "Identical → Actual order" is due to the cell diameter of n-th cup b_n^c which is the average of those of the n-th and (n-1)-th disk cell radius, b_n^d and b_{n-1}^d, where $b_{n-1}^d > b_n^d$ [6]. As shown in the table, the frequencies at these three points along the structure are close enough to assure that all of the cells are within the tuning range considering the cell-to-cell scattering described in the above section.
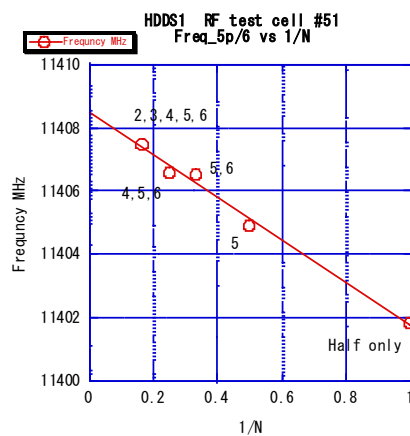
021220

HDDS1 RF test cell #51
Freq_5p/6 vs 1/N

Fig. 18.   Measured frequency as function of inverse of the total number of cells, N.

15

Table 3. Estimation of 5π/6 mode frequency at 45 degree C in vacuum. All units are in MHz.

Cell number	Cell #3	Cell #31	Cell #51
Measurement	11401.8	11418.5	11408.4
N2 → Vacuum	+3	+3	+3
Meas. temp→ 45degC	-4	-4	-4
Identical → Actual order	+21.2	+6.4	+16.3
Estimated at 45C in VAC	11422.0	11423.9	11423.7

6. Summary

By improving the milling tool shape and the tool passage, the tangential angle discontinuities were firmly suppressed within the specification. It is to be noted that the intersection angle between R0.5 to flat at the rim of the slot edge actually increased to 8 degrees, which was larger than the nominal value of the previous structure, H60VG3N-6C. The dimensions such as "2a" and "2b" were well controlled within the tolerance of ±20μm. Especially almost all of the "2b" dimensions were within ±5μm. In addition and probably more important to be noted is that the dimensions determined by the milling were controlled within ±10μm when averaging the four values in a cell. Reflecting these dimensional qualities in turning and milling, the frequency scattering was found to be within 5MHz or better. The absolute accelerating-mode frequency was found to meet the design value within a few MHz without any additional correction was made.

7. Acknowledgments

8. References

1. T. Higo et al., JLCX-005, Jan. 2003.
2. Discussions in ISG8, SLAC, June 2002.
3. FUJINON Inc., an interferometer, FUJINON F601.
4. Mitsutoyo co. ltd., Formtracer CS-5000.
5. Keyence co., Laser Microscope, VK-8500.
6. Z. Li, presentation in ISG8, SLAC, June 2002.